# Performance Comparison of Protonic and Sodium Phosphomolybdovanadate Polyoxoanion Catholytes Within a Chemically Regenerative Redox Cathode Polymer Electrolyte Fuel Cell

David B. Ward, Natasha L.O. Gunn, Nadine Uwigena and Trevor J. Davies*

Department of Natural Sciences, Faculty of Science & Engineering, University of Chester, Thornton Campus, Thornton Science Park, Pool Lane, Ince, Chester, CH2 4NU, United Kingdom.

*Corresponding Author:

Email: t.davies@chester.ac.uk

Tel: +44(0)1244 512297

Fax: +44(0)1244 511300

**To be submitted to *the Journal of Power Sources***

## Abstract

The direct reduction of oxygen in conventional polymer electrolyte fuel cells (PEFCs) is seen by many researchers as a key challenge in PEFC development. Chemically regenerative redox cathode (CRRC) polymer electrolyte fuel cells offer an alternative approach via the indirect reduction of oxygen, improving durability and reducing cost. These systems substitute gaseous oxygen for a liquid catalyst that is reduced at the cathode then oxidised in a regeneration vessel via air bubbling. A key component of a CRRC system is the liquid catalyst or catholyte. To date, phosphomolybdovanadium polyoxometalates with empirical formula $H_{3+n}PV_nMo_{12-n}O_{40}$ have shown the most promise for CRRC PEFC systems. In this work, four catholyte formulations are studied and compared against each other. The catholytes vary in vanadium content, pH and counter ion, with empirical formulas $H_6PV_3Mo_9O_{40}$, $H_7PV_4Mo_8O_{40}$, $Na_3H_3PV_3Mo_9O_{40}$ and $Na_4H_3PV_4Mo_8O_{40}$. Thermodynamic properties, cell performance and regeneration rates are measured, generating new insights into how formulation chemistry affects the components of a CRRC system. The results include the best CRRC PEFC performance reported to date, with noticeable advantages over conventional PEFCs. The optimum catholyte formulation is then determined via steady state tests, the results of which will guide further optimization of the catholyte formulation.

## Highlights

- Four polyoxometalate catholytes are investigated in a regenerative fuel cell.
- The catholytes vary in terms of vanadium content, counter ions and pH.
- Thermodynamic properties, cell performance and regeneration rates are reported.
- Steady state system performance generates insights into formulation optimization.


## Keywords

Polymer electrolyte fuel cells; Chemically regenerative redox cathode; Regeneration; Catholyte; Phosphomolybdovanadate polyoxometalate; Heteropolyanion.

# 1. Introduction

Issues surrounding cost and durability continue to inhibit the widespread commercialisation of polymer electrolyte fuel cells (PEFCs) across both stationary power and automotive sectors [1,2]. The main cause of these problems is the direct 4-electron reduction of oxygen at the cathode. Due to relatively slow kinetics [3,4], conventional PEFCs require high platinum loadings to catalyse the oxygen reduction reaction (ORR), increasing the cost of the membrane electrode assembly (MEA) [5]. Even with increased amounts of catalyst, the oxygen reduction reaction can be the source of more than half the voltage loss in a PEFC system [6]. The presence of air at the cathode is also a key component in the major mechanisms of fuel cell degradation, including high voltage transients at cell start-up and shut-down [7, 8] and chemical degradation of membranes via highly oxidative species [9, 10].

Figure 1 illustrates the alternative approach of chemically regenerative redox cathode (CRRC) PEFCs, which utilise the indirect reduction of oxygen [11]. The anode is essentially identical to that of a conventional PEFC, with hydrogen gas supplied via a flow field through a gas diffusion layer onto a catalyst (platinum) coated membrane. The difference lies on the cathodic side of the cell, where a liquid catalyst (catholyte) circulates between the cathode and an air-liquid contacting reactor called the “Regenerator”. At the cathode, the electrochemical reduction of the catholyte is relatively facile and can be conducted at carbon rather than platinum, significantly reducing the cost of the MEA. Subsequent catholyte re-oxidation, via air bubble infusion, is conducted within the regenerator, where oxygen is reduced to water. The result is a fuel cell where gaseous air never enters the cathode, eliminating the major PEFC degradation mechanisms. In addition, the catholyte ensures the membrane remains well hydrated, negating the requirement for gas humidification and allowing operational temperatures greater than 80°C.

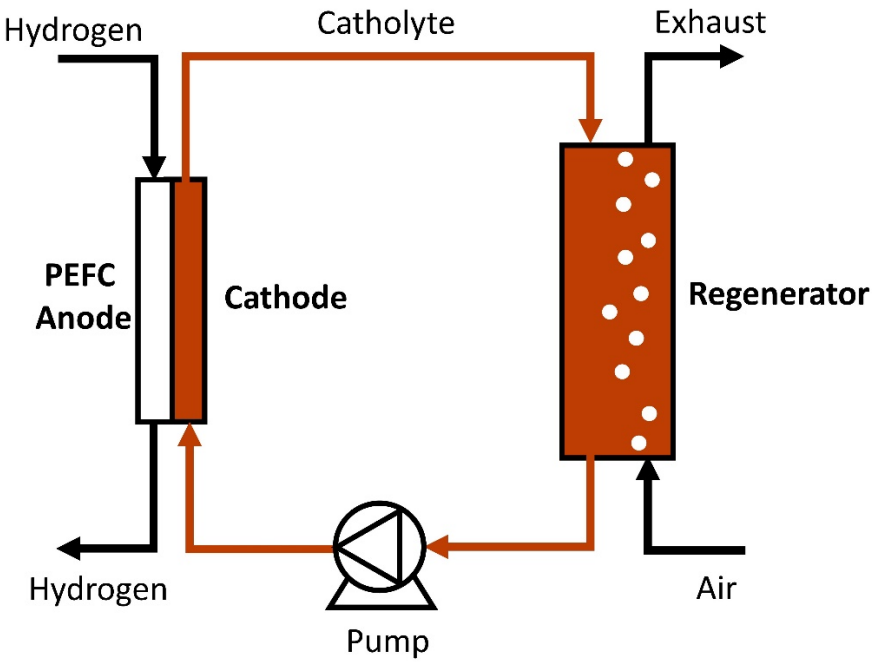


**Figure 1.** Schematic diagram of a CRRC PEFC system.

Posner first proposed the CRRC concept in 1955, using a bromine/bromide redox couple for the catholyte [12]. In the early 1980s, the Ford Motor Company were one of the first to employ a vanadium(IV)/vanadium(V) couple in a CRRC catholyte, although they struggled to replicate the performance of conventional PEFCs [13,14]. Since then, several researchers and organisations have further developed the concept using a range of catholyte redox chemistries including $Fe^{2+}/Fe^{3+}$, $HNO_3$/NO and polyoxometalates (POMs) [11, 15-21]. A notable contribution was from ACAL Energy Ltd, who operated a CRRC PEFC for over 10,000 hours on an automotive test cycle with negligible loss in cell performance and almost commercialised their system [22]. The most advanced CRRC PEFC system reported to date used a POM-vanadium(IV)/vanadium(V) system and disclosed headline performance figures of 0.90 V at 0.2 A $cm^{-2}$, 0.72 V at 1 A $cm^{-2}$ and a maximum power of 1.00 W $cm^{-2}$ [21]. This is comparable with that of conventional fuel cells [23], suggesting the platinum-free technology could be close to market deployment.

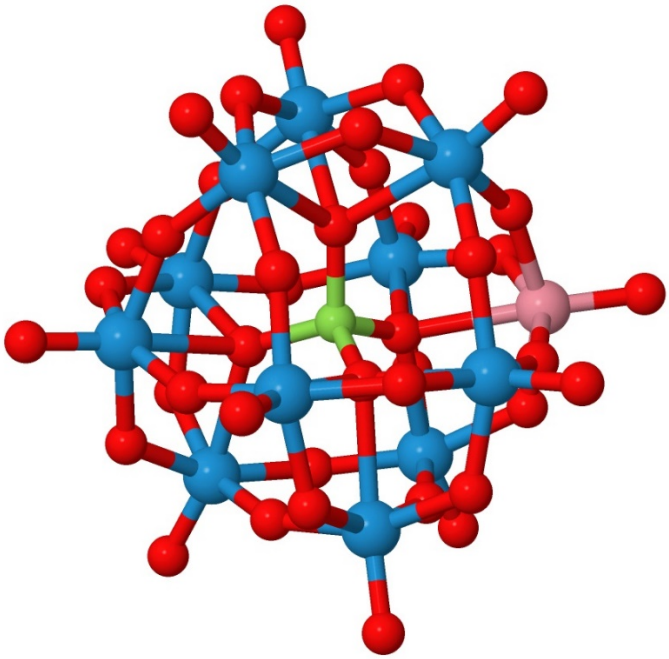

**Figure 2.** Representation of the α-keggin structure $[PV_1Mo_{11}O_{40}]^{4-}$ with phosphorous in green, molybdenum in blue, vanadium in pink and oxygen in red.

A key component of the CRRC PEFC system is the catholyte. An effective catholyte must possess several properties: a relatively high redox potential to ensure high thermodynamic efficiency; good ionic conductivity and facile electrode kinetics to allow for acceptable cell performance; and fast regeneration kinetics to maintain a reasonable operating voltage [11]. To date, the most developed CRRC catholytes are aqueous solutions of polyoxometalates (POMs) incorporating keggin-type mixed-addenda heteropolyanions of general formula $PV_nMo_{12-n}O_{40}^{(3+n)-}$, denoted HPA-*n* [24]. The $\alpha$-keggin structure is shown in Figure 2 and consists of a central tetrahedral $PO_4$ ion surrounded by twelve $MO_6$ distorted octahedra, where M is the metal (in this case either Mo or V). For a fully oxidised HPA-*n*, the Mo and V addendum atoms are in oxidation states 6 and 5, respectively, and the counter cations are often protons or a mixture of protons and Group 1 metal ions [25]. CRRC PEFC systems with such POM-based catholytes utilise the vanadium(V)→(IV) electrochemical reduction and the vanadium(IV)→(V) chemical oxidation. Although these catholytes often have the empirical formula of a keggin molecule, for $n>1$ they exist as an equilibrium mixture of keggins, free vanadium, free phosphate and other ionic species [26-29]. For example, a fully oxidised aqueous solution of

empirical formula $H_6PV_3Mo_9O_{40}$ contains $VO_2^+$, phosphate and the keggins $[PV_4Mo_8O_{40}]^{7-}$, $[PV_3Mo_9O_{40}]^{6-}$, $[PV_2Mo_{10}O_{40}]^{5-}$ and $[PV_1Mo_{11}O_{40}]^{4-}$ [21]. The speciation depends on the total POM concentration, pH, temperature and additional cations present in solution [26-28]. Reduced solutions of $H_6PV_3Mo_9O_{40}$ also contain vanadium(IV) species, present as $VO^{2+}$ and/or reduced keggins. Consequently, the cathode reduction reaction involves the reduction of vanadium(V) to (IV) in both free and keggin bound forms, where $1 \le n \le 4$ and $0 \le m \le 4$ [30]:

$$\left[H_{n+m-1}PV_m^{IV}V_{n-m}^{V}Mo_{12-n}O_{40}\right]^{4-} + e^- + H^+ \leftrightarrow \left[H_{n+m}PV_{m+1}^{IV}V_{n-m-1}^{V}Mo_{12-n}O_{40}\right]^{4-} \quad (1)$$

$$VO_2^+ + e^- + 2H^+ \leftrightarrow VO^{2+} + H_2O \quad (2)$$

In contrast, the catholyte oxidation reaction occurring in the regenerator only involves reduced keggins [31,32]. The reaction is thought to follow a 3 or 4-electron pathway involving an intermediate activated complex [33], but for simplicity can be written as:

$$\left[H_{n+m-1}PV_m^{IV}V_{n-m}^{V}Mo_{12-n}O_{40}\right]^{4-} + \frac{1}{4}O_2 \leftrightarrow \left[H_{n+m-2}PV_{m-1}^{IV}V_{n-m+1}^{V}Mo_{12-n}O_{40}\right]^{4-} + \frac{1}{2}H_2O \quad (3)$$

Despite the importance of the catholyte formulation, the literature on POM-formulation effects in CRRC PEFCs is sparse. The only substantial study of formulation was conducted by Matsui et al, who investigated $H_3PMo_{12}O_{40}$, $H_5PV_2Mo_{10}O_{40}$ and $H_6PV_3Mo_9O_{40}$ at different temperatures and concentrations [19]. They also varied pH in dilute solutions (0.01 M) of $H_6PV_3Mo_9O_{40}$ and found pH played a key role in system performance. Although the researchers found 0.3 M $H_6PV_3Mo_9O_{40}$ at 80°C gave the optimum system performance, their best peak power density was ~40 mW $cm^{-2}$, much lower than that of conventional fuel cells. Recently, Gunn et al reported a high performance CRRC PEFC using 0.3 M $H_6PV_3Mo_9O_{40}$ as the catholyte, achieving a peak power density of 1000 mW $cm^{-2}$ [21]. In addition, the researchers established several key measurement techniques to assess the catholyte over a range of reduction levels, with focus on catholyte redox potential, regeneration rate,

cell power density and steady state system performance. In the present study, the same methodology and high-performance system is used to investigate the effect of three key parameters on the catholyte, namely vanadium content, pH and sodium content. First, a catholyte with empirical formula $H_6PV_3Mo_9O_{40}$ (HV3) is compared with $H_7PV_4Mo_8O_{40}$ (HV4), both catholytes having concentration 0.3 M. HV4 is expected to demonstrate faster regeneration kinetics due to its more favourable speciation [32]. In addition, the extra vanadium in HV4 is an increase of 33% in concentration of electroactive species compared to HV3, so should result in a higher exchange current density and improved fuel cell performance. Second, the sodium equivalents of HV3 and HV4, with empirical formulas $Na_3H_3PV_3Mo_9O_{40}$ (NaV3) and $Na_4H_3PV_4Mo_8O_{40}$ (NaV4), are investigated. This generates insights into the effects of pH and sodium content in the high performance CRRC system, with pH affecting POM thermodynamics, cell performance and regeneration kinetics. In addition, the study reports the first thorough investigation of three new POM formulations, 0.3 M HV4, 0.3 M NaV4 and0.3 M NaV3. The results provide a concise overview of the challenges faced in formulating CRRC catholytes and offer guidance for future research and development.

## 2. Experimental

### *2.1 Catholyte Synthesis and Analysis*

The synthesis of HV3 and HV4 catholytes followed the “Metallomax” procedure disclosed in Ref. [34] and used deionised water (with a resistivity of 18.2 MΩ cm), $V_2O_5$ powder (99.2%, Alfa Aesar, UK), Mo powder (99.9%, Alfa Aesar, UK), $H_3PO_4$ (85.0%, Sigma Aldrich, UK) and $MoO_3$ (99.5%, Alfa Aesar, UK). NaV3 and NaV4 catholytes were produced from their HV3 and HV4 counterparts via the addition of NaOH (98%, Alfa Aesar, UK). Concentration was evaluated gravimetrically using a 25 mL density jar (Jaytec Glass Ltd, UK) and pre-determined density vs. concentration calibration curves. Table S1, in the supporting information, gives the density of each catholyte at 0.3 M and 20°C.

Fully oxidised samples of each catholyte (achieved electrochemically by reverse operation of the fuel cell) were submitted for $^{31}P$ NMR analysis to determine the speciation in aqueous solution [27,28]. Further details and spectra are given in the Supporting Information (see Figure S1).

## *2.2 CRRC Fuel Cell Test System*

All fuel cell tests conducted within this study were performed using an integrated CRRC fuel cell test stand (ACAL Energy, UK) as reported previously [21]. The catholyte flow rate through the cell was 140±10 mL $min^{-1}$ and corresponded to a pumping pressure of 580±20 mbar (through a 5×5 cm cathode). The anode was operated "dead-ended" at a hydrogen pressure of 0.57 barg, with occasional purges to remove excess water. The system (cell, catholyte and regenerator) temperature was maintained at 80±2°C. The catholyte redox potential was continuously monitored using an in-line redox probe identical to that reported previously [35]. A HCP 803 potentiostat (Bio-Logic, France) was used to control and monitor current load and cell voltage. During catholyte regeneration, the air flow rate through the bubbling device, a porous glass sparge (ROBU Glasfilter-Geraete GmbH, Germany), was 1 L $min^{-1}$.

Sequentially, 300 mL of each catholyte (0.3 M concentration) was tested in the system. In each case, this equated to 0.09 moles of POM catholyte. However, in terms of vanadium this gave 0.27 moles for the HV3 and NaV3 and 0.36 moles for the HV4 and NaV4. To minimise cross contamination between tests, each catholyte was evacuated from the system (pump ran in reverse) and the wetted interior thrice rinsed using deionized water (resistivity of 18.2 MΩ cm).

Prior to each day of testing, system catholyte concentration was gravimetrically determined offline and adjusted accordingly by deionized water addition or evaporation. Throughout all tests, glass coil reflux condensers on the test rig successfully maintained catholyte concentrations to within ±10% the target value (i.e. 0.3±0.03 M). In general, slightly more water escaped through the regenerator's condensers than was formed by the regeneration reaction. Consequently, over an 8-hour testing period the POM concentration increased by an average of 5%.

## 2.3 Cell Build

Cell construction was identical to that used previously [21] and is briefly described here. The MEA was a reinforced Gore Primea (W. L. Gore & Associates, Inc., USA) with an anode active area of 5 × 5 cm (25 $cm^2$) and a platinum loading of 0.4 $mg.cm^2$. A 34BC (SGL Group GmbH, Germany) gas diffusion layer was adjacent to the anode catalyst layer followed by a graphite plate with a serpentine flow field. The cathode side of the MEA was naked and adjacent to a GFD 2.5EA graphite felt electrode (SGL Carbon GmbH, Germany) followed by a graphite plate that provided a 1 mm deep well for the felt to occupy (the felt compression corresponding to 3.5-4 bar compression pressure on the active area). The cell components were sandwiched between gold plated copper current collectors and stainless-steel end plates.

## 2.4 Catholyte Reduction Curves

The level of reduction of the catholyte (analogous to the "state of charge" of a battery) is a key parameter when operating a CRRC system and is equal to the fraction of vanadium(IV), $\theta$, where $\theta$ is defined as the total concentration of vanadium in the "4+" oxidation state divided by the total concentration of vanadium:

$$\theta = \frac{[\text{vanadium(IV)}]}{[\text{vanadium}]} \tag{4}$$

Each catholyte was electrochemically oxidised to less than 1% of vanadium(IV) (confirmed via UV-Vis spectroscopy) using a sacrificial cell. The catholyte was then gently reduced in the CRRC test rig whilst passing nitrogen gas through the regenerator (to avoid chemical oxidation via $O_2$) and recording the redox probe and open circuit voltages. Assuming 100% current efficiency, a plot of open circuit (or redox probe) voltage vs. $\theta$ was generated for each catholyte.

## 2.5 Cell Performance Testing at Various Catholyte Oxidation States

Catholyte cell performance was evaluated via current-voltage ($I$-$V$) curves and electrochemical impedance spectroscopy. Following the same procedure in Ref. [21], $I$-$V$ curves were generated (at a

current sweep rate of 0.5 A $s^{-1}$) for each catholyte at five reduction levels: $\theta$ = 0.05, 0.25, 0.45, 0.65 and 0.85. Table 1 gives the target vanadium(IV) fraction and respective redox potentials for each catholyte.

All $I$-$V$ and impedance tests were carried out for two cell builds and duplicate test were carried out per build. In the interests of consistency, an anode recovery procedure (described in Ref. [21]) was performed prior to each test.

## *2.6 Regeneration Performance Testing*

Regeneration performance of each catholyte was assessed using the 'Sweep' method described in Ref. [21]. Each catholyte was electrochemically reduced to $\theta \approx 0.8$ in the CRRC rig under nitrogen. The regenerator then supplied air to the system and the rate of catholyte oxidation was monitored via recording the catholyte potential over a period of time. Using the appropriate catholyte reduction curve, this was expressed as a plot of $\theta$ vs. time, the gradient of which represents a quantity of electrons lost by vanadium(IV) centres per unit time. Hence, for each catholyte and each value of $\theta$, a regeneration current, $I_R$, can be determined using:

$$I_R = \frac{dQ_R}{dt} = V\left[\mathrm{POM}\right] nF \frac{d\theta}{dt} \tag{5}$$

where $Q_R$ is the equivalent charge passed due to the oxidation reaction, $t$ is time, $V$ is the volume of catholyte, [POM] is the concentration of POM (i.e. the concentration of the empirical formula), $n$ is the number of vanadium centres in the POM empirical formula (e.g. for HV4, $n$ = 4), and $F$ is Faraday's constant. Using this approach, $I_R$ can be directly related to the load applied to the fuel cell, $I$, which allows the prediction of cell performance when the system is in a steady state (i.e. when $I_R$ = $I$).

## *2.7 Ex situ Conductivity and pH Analysis*

Samples of each catholyte were collected over a range of vanadium(IV) fractions (i.e. 0.05, 0.25, 0.45, 0.65 and 0.85) and kept under a nitrogen atmosphere. The conductivity, pH and redox potential of

each sample was then analysed at 22°C and 80°C (±2°C). Measurements were taken using a pHenomenal CO1300L conductivity meter (VWR International, UK) and an 827 pH Lab pH meter (Metrohm, UK). Redox potential was measured between a mercurous sulphate reference electrode arrangement (as described above) and a JP945 graphite rod (Merson UK, UK) using a 117 True RMS Multimeter (Hanna Instruments, UK).

## 3. Results and Discussion

### *3.1 Thermodynamic Properties and Ex-Situ Measurements*

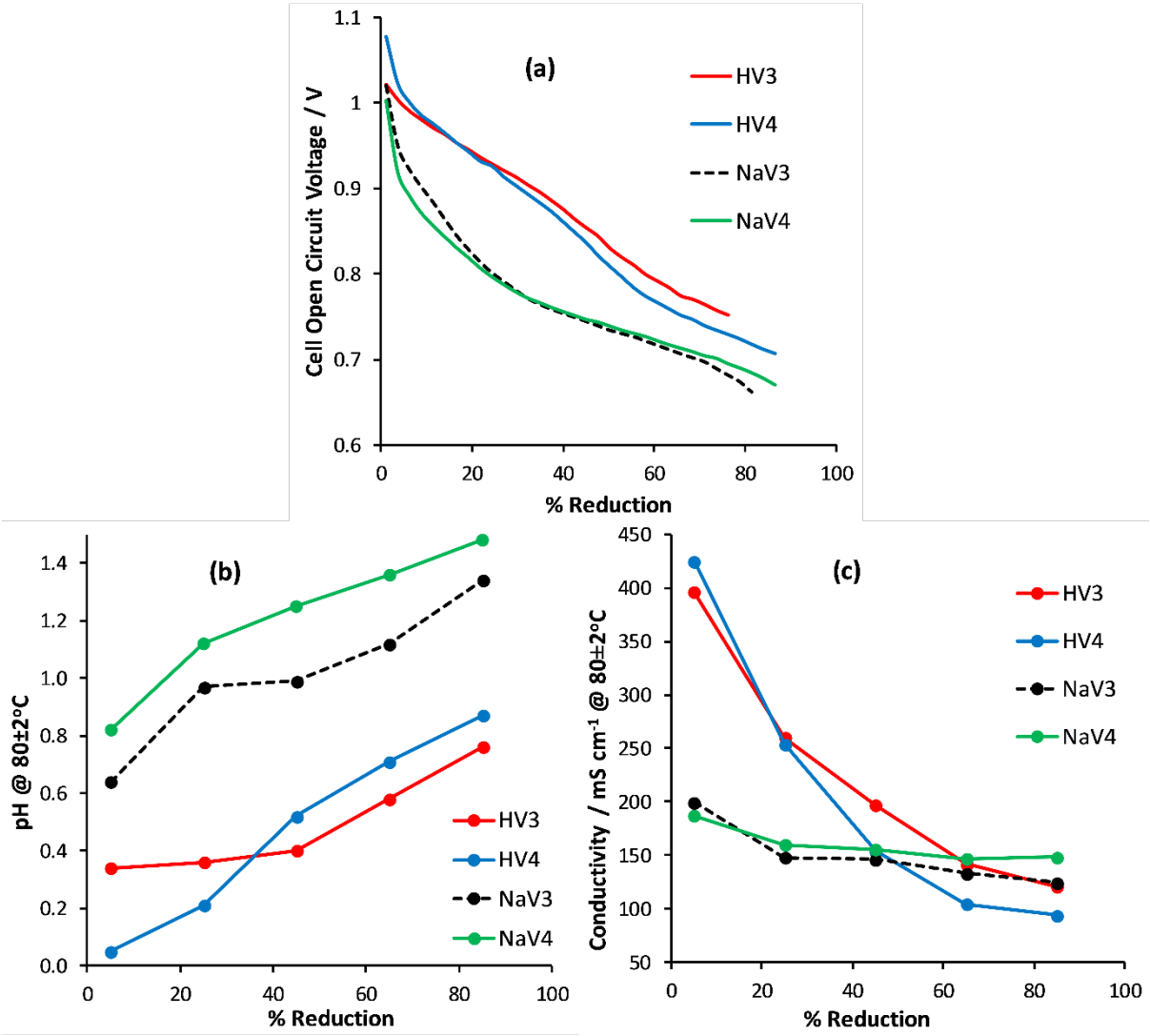


**Figure 3.** (a) Cell open circuit voltage obtained with various catholytes over a range of reduction levels at 80°C and the corresponding catholyte (b) pH and (c) conductivity measurements.

Figure 3a illustrates reduction curves for the four catholytes (HV3, HV4, NaV3 and NaV4) in the CRRC test rig at 80°C. The protonic catholytes, HV3 and HV4, have a similar profile that is on average approximately 100 mV greater than the sodium catholytes (which also possess a similar profile to each other) for a given reduction level. A corresponding plot obtained using the in-line redox probe is shown in Figure S2 (Supporting Information) and is almost identical, suggesting the potential of the hydrogen anode is constant for all four catholytes. As expected, open circuit voltage (OCV) decreases as the level of reduction increases, whereas the increase in vanadium content, from the V3 to V4 formulations, appears to have little effect over most of the plot. Odyakov et al. performed similar experiments on 0.01 M solutions of HV3 and HV4 and found comparable results, with little difference between the two protonic POMs [30]. The reduction profiles in Figure 3a were fitted to 6$^{th}$ order polynomial curves and used in subsequent calculations (to determine $I_R$ at different values of $\theta$).

The trends in Figure 3a can be largely explained by Figure 3b, which shows the results of ex-situ pH measurements (at 80°C) for the catholytes over a range of reduction levels. For all the catholytes, the pH increases with the level of reduction, where the change in pH from 0 to 100% reduced is approximately 0.9 units (with the exception of HV3, for which the change is approximately 0.5 units), in good agreement with previous work on 0.01 M solutions of HV3and HV4 [30]. The main cause for the increase in pH is the presence of free vanadium in the aqueous solutions [30,32]. Although $PV_nMo_{12-n}O_{40}$ keggins undergo 1 electron, 1 proton reductions [31], free vanadium(V) undergoes a 1 electron, 2 proton reduction, thus consuming twice as many protons than that delivered from the hydrogen oxidation reaction. Consequently, catholyte pH increases with reduction, the profile of which depends on the speciation in the reduced solution. The difference in pH between protonic and sodium POMs is also expected from the synthesis method. For example, fully oxidised HV4 and NaV4 differ by approximately 0.8 pH units. Given that 0.3 M NaV4 was synthesised by adding NaOH to 0.3 M HV4, such that the concentration of NaOH in the sodium POM solution was 1.2 M, we would expect a difference of approximately 1 pH unit between the two catholytes. The difference in pH between fully oxidised HV3 and NaV3 is less than their V4 analogues (approximately 0.5 units)

because less NaOH was added in the synthesis of NaV3. Note that, although the trends in Figure 3a appear to be Nernstian, with the difference between catholytes largely caused by pH effects, it is not possible to fit a meaningful Nernst-type equation to the experimental data due to the complexity of the system [21].

Figure 3c illustrates plots of conductivity vs. reduction level (at 80°C) for the four catholytes. At low levels of reduction, the protonic POMs have double the conductivity of their sodium counterparts, most likely a result of the difference in pH. Consequently, as the protonic POMs are reduced and their pH increases, their conductivity drops dramatically. In contrast, the decrease in conductivity for the sodium POMs is much shallower, suggesting the free vanadium / keggin / phosphate species and extra sodium cations make a significant contribution to the ionic current. Beyond 40% reduced, there is little difference in conductivity between the four catholytes.

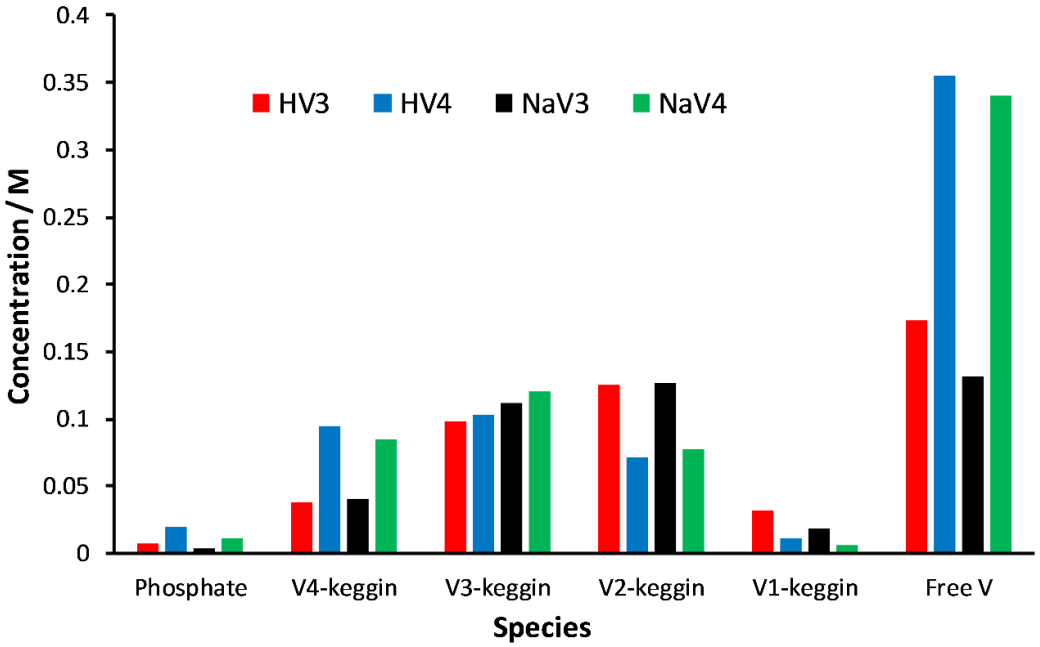


**Figure 4.** Estimated concentrations of species present in fully oxidized catholytes at 80°C (determined from $^{31}$P NMR), where the catholyte concentration is 0.3 M.

To provide an indication of the speciation in the catholytes, fully oxidised samples underwent $^{31}$P NMR analysis over a range of temperatures. Example spectra are given in the Supporting Information. Peak analysis followed that of Pettersson and co-workers [27,28], from which it was

possible to estimate concentrations of different species: free vanadium(V) or $VO_2^+$ (Free V); $PV_1Mo_{11}O_{40}$ keggins (V1-keggin); $PV_2Mo_{10}O_{40}$ keggins (V2-keggin); $PV_3Mo_9O_{40}$ keggins (V3-keggin); $PV_4Mo_8O_{40}$ keggins (V4-keggin); and free phosphate (Phosphate). The speciation for each catholyte at 80°C is illustrated in Figure 4.

The general reaction governing speciation in solutions of $[H_{n-1}PV_nMo_{12-n}O_{40}]^{4-}$ (i.e. fully oxidised POM) shows how vanadium(V) can reversibly enter and leave a keggin species [36]:

$$\begin{aligned}&(13-n)\left[H_{n-1}PV_nMo_{12-n}O_{40}\right]^{4-} + 16H^+ \rightleftarrows \\ &(12-n)\left[H_{n-2}PV_{n-1}Mo_{13-n}O_{40}\right]^{4-} + 12VO_2^+ + H_3PO_4 + 12H_2O\end{aligned} \qquad (6)$$

This suggests that an increased amount of vanadium in the POM empirical formula should lead to keggins with increased vanadium content, as observed in Figure 4 when comparing the V3 POMs with their V4 counterparts. This is most noticeable for the V4-keggin species, with the V4 POMs containing double the amount of V4-keggin than the V3 POMS. Likewise, increased acidity (lower pH) should lead to more free vanadium, which is also seen in Figure 4 when comparing HV3 with NaV3 and HV4 with NaV4.

## *3.2 Cell Performance*

Figure 5 illustrates fuel cell performance curves for the HV4 catholyte (0.3 M concentration) at a range of reduction levels. As expected, the position of the current density-voltage (*i*-*V*) curves in Figure 5a depends on the catholyte potential (i.e. open circuit potential), which decreases as the level of reduction increases. The *i*-*V* curves display a more linear profile than that for conventional PEFCs, with no significant activation loss due to the facile reduction kinetics of the catholyte. On closer inspection, the five *i*-*V* curves are not quite parallel. The gradient increases with the level of reduction, most likely caused by the increase in pH and the decrease in conductivity of the catholyte [21]. The corresponding power curves in Figure 5b also demonstrate how peak power is highly dependent on the catholyte reduction level.

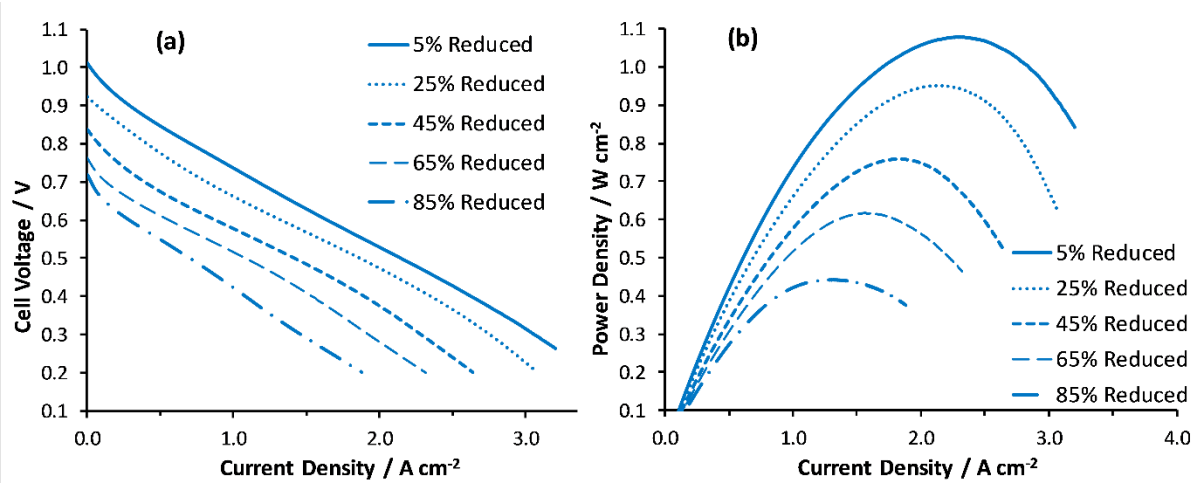


**Figure 5.** (a) *i-V* and (b) corresponding power density curves generated with 0.3 M HV4 at varying levels of reduction.

The performance of the highly oxidised HV4 catholyte in Figure 5 is impressive and represents the best CRRC fuel cell performance reported to date, as demonstrated in Table 2, with headline figures of 0.927 V at 0.2 A $cm^{-2}$, 0.736 V at 1 A $cm^{-2}$ and a maximum power of 1.078 W $cm^{-2}$. The performance also compares favourably against state of the art conventional PEFCs with similar MEAs, with noticeably higher cell voltages at 0.2 and 1.0 A $cm^{-2}$ gained using half the platinum loading of the conventional PEFC [23]. Furthermore, the HV4 CRRC PEFC (5% reduced) exceeds two key Department of Energy (DOE) 2020 transportation targets [37]: rated power (1078 vs. 1000 mW $cm^{-2}$) and performance at 0.8 V (708 vs. 300 mA $cm^{-2}$). The latter is particularly impressive and demonstrates the benefit of replacing the slow oxygen reduction kinetics with a much faster $V^{5+/4+}$ redox couple. Indeed, a similar result was recently reported by Park and co-workers, who achieved ~600 mV at 0.8 V with their $NO_3^-$/NO CRRC system [17]. Although the HV4 CRRC PEFC does not meet the DOE target for Pt content (0.4 vs. 0.125 mg $cm^{-2}$), the Pt is only required on the anode and, given that 0.4 mg $cm^{-2}$ is generally considered a high loading for the hydrogen oxidation reaction [38], decreasing the Pt content by a factor of 4 is not expected to noticeably impact cell performance. Thus, if low catholyte reduction levels can be maintained during operation, a CRRC PEFC system can be competitive with conventional PEFCs and meet key DOE targets. The corresponding *i-V* and power curves for the HV3, NaV3 and NaV4 catholytes over a range of reduction levels are given in

the supporting information (Figure S3) and show the same trends, although with less impressive performance.

Figure 6 compares *i-V* and power density curves for each catholyte at a vanadium(IV) fraction of 0.45. The relative positioning of the protonic and sodium POM curves reflect that in Figure 3a and are mostly influenced by the open circuit voltage, with the NaV3 and NaV4 *i-V* curves approximately 100 mV lower than HV3 and HV4 for a given current density. Consequently, the protonic POMs achieve higher cell power densities, with HV4 slightly better than HV3. Below 1 A $cm^{-2}$, the vanadium content has little effect on the performance of the CRRC cell. However, at higher current densities both the NaV4 and HV4 catholytes display better performance than their V3 analogues. This is most likely a concentration effect as the V3 catholytes contain less vanadium so will have a lower limiting current density than the V4 POMs. For example, at 2 A $cm^{-2}$, where there is a noticeable difference between V3 and V4 catholytes, the utilization rates (for 45% reduced catholyte at a flow rate of 140 mL $min^{-1}$) are 0.45 and 0.34 for the V3 and V4 catholytes, respectively.

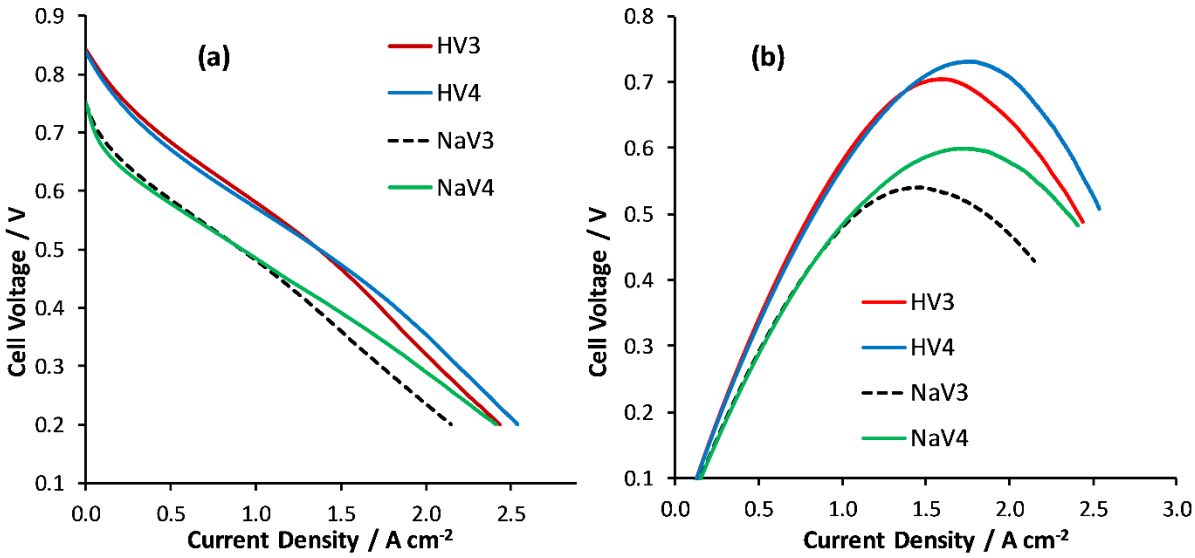


**Figure 6.** (a) *i-V* and (b) corresponding power density curves generated with four catholyte formulations (0.3 M concentration), each 45% reduced.

Electrochemical impedance measurements were conducted at 1 A $cm^{-2}$ on all four catholytes, where each catholyte was 65% reduced. The corresponding cell high frequency resistance (HFR) values are

given in Table 2. The ranking of catholytes in terms of HFR almost inversely correlates with the conductivity measurements in Figure 3c. The presence of sodium cations appears to decrease the cell's area specific ohmic resistance by at least 10 $\Omega$ cm$^2$. However, all the CRRC PEFC HFR values are at least double that for high performance conventional PEFCs (45-55 $\Omega$ cm$^2$) [23], suggesting significant performance gains can be made by further optimizing the cell build/components. A similar problem has been addressed by researchers working with flow batteries, which use comparable electrolytes to POM. For example, vanadium redox flow batteries (VRFBs) made with graphite felt electrodes (the conventional electrode material) have relatively high cell ohmic resistances that limit the peak power density, with 311 mW cm$^{-2}$ being the highest value reported to date [39]. In 2012, researchers at the University of Tennessee assembled VRFBs using carbon paper electrodes (instead of graphite felt) combined with serpentine flow fields and obtained a peak power density of 557 mW cm$^{-2}$ [40]. This was followed by electrode pre-treatments, membrane and flow field optimization to further increase power density to 767 and 1290 mW cm$^{-2}$ [41,42]. Their work triggered an abundance of studies with carbon paper and carbon cloth electrodes, developing high performance VRFBs [43]. In particular, Zhao and co-workers developed KOH-activated carbon paper and cloth electrodes, achieving record VRFB performance values [44,45]. Moreover, one of the best performing cells reported in the literature, with a peak power density of 1460 mW cm$^{-2}$ and HFR value of 75 $\Omega$ cm$^2$, was a hydrogen-bromine redox flow battery with carbon paper electrodes [46]. This suggests using a thinner, less compressible electrode material like (pre-treated) carbon paper or carbon cloth in combination with an optimized flow field should result in noticeably better fuel cell performance than the graphite felt cell used in this study.

### *3.3 Regenerator Performance*

Figure 7a illustrates plots of open circuit voltage vs. time, obtained from regeneration sweeps with each of the four catholytes. As observed, the regeneration of HV3 appears to take much longer than

the other three catholytes. The corresponding plots of regeneration current vs. reduction level are shown in Figure 7b. These illustrate a stark difference between the sodium and protonic POMs, with NaV4 and NaV3 capable of much higher regeneration rates than HV3 and HV4. These differences have a marked impact on the performance of the CRRC PEFC system. For example, the maximum current a CRRC fuel cell can produce for a prolonged period of operation is the maximum regeneration current, which is less than 20 A for the HV3 system. The same figure for the NaV4 system is almost 70 A. By extrapolating to zero regeneration current, Figure 7b also provides information on the maximum open circuit voltage achievable for each catholyte via regeneration. The sodium POMs can be regenerated to less than 20% reduced whereas 40-50% of the vanadium in the protonic POMs is not recoverable. Thus, the sodium POMs are able to utilise much more of their vanadium content. Having four, rather than three, vanadium atoms in the empirical formula also appears to improve regeneration performance, in agreement with the results of Zhizhina et al [32].

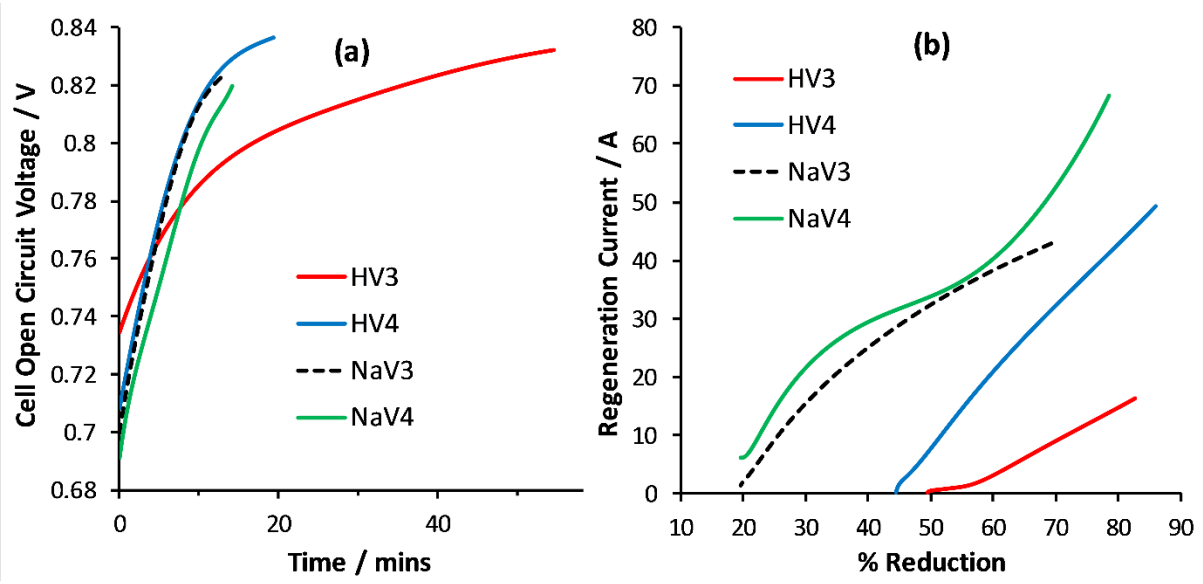


**Figure 7.** (a) Regeneration sweeps for 4 catholyte formulations and (b) the corresponding regeneration current curves

Given the reaction of reduced keggins with oxygen (to form oxidised keggins and water) is expected to proceed via a 3 or 4 electron pathway with reduced V3 and V4 keggins [33,47,48], catholytes containing relatively large amounts of V3 and V4 keggins would be expected to display more favourable regeneration kinetics. Thus, according to the $^{31}$P NMR results in Figure 4, HV4 and NaV4

should have similar regeneration performance. However, the speciation of reduced $PV_nMo_{12-n}O_{40}$ systems is complicated [26]. First, for low levels of reduction, vanadium(V) exists as free and keggin-bound, so electrochemical reduction can generate either free vanadium(IV) ($VO^{2+}$) or reduced keggin species. Second, the smaller and more highly charged $VO^{2+}$ species (vs. $VO_2^+$) can significantly alter the keggin/free vanadium dynamic equilibrium, in some cases reducing the concentration of keggin species by expulsion of vanadium(IV) [49]:

$$\begin{aligned}&(13-m)\left[H_{2m-1}PV_m^{IV}Mo_{12-m}O_{40}\right]^{4-} + 28H^+ \\ &(12-m)\left[H_{2m-3}PV_{m-1}^{IV}Mo_{13-m}O_{40}\right]^{4-} + 12VO^{2+} + H_3PO_4 + 24H_2O\end{aligned} \quad (7)$$

For example, when studying the 50% reduced $PV_{1.8}Mo_{10.2}O_{40}$ system, Selling et al. found that below pH 1, vanadium(IV) was almost exclusively present as $VO^{2+}$, with negligible reduced V-keggins [50]. As the pH increased, the concentration of reduced keggins (e.g. $PV^{IV}Mo_{11}O_{40}$) increased at the expense of $VO^{2+}$, and above pH 2, the majority of vanadium(IV) was found in keggin species. It is likely the $PV_3Mo_9O_{40}$ and $PV_4Mo_8O_{40}$ systems in this work follow the same trends, with low pH favouring free vanadium(IV) and inhibiting the formation of reduced keggin species. Consequently, pH has a large effect on regeneration rates and the sodium POMs perform much better than their protonic analogues.

### *3.4 Steady State System Performance*

In a CRRC fuel cell system, steady state operation is achieved when the cell current, $I$, equals the regeneration current, $I_R$ [21]. Figure 7b can be used to predict the catholyte reduction level for a given steady state condition. For example, the HV4 system producing a current of 25 A (1 A $cm^{-2}$) at steady state will have a catholyte reduction level of 63.5% (obtained via interpolation of Figure 7b). Referring to Figure 3a, this corresponds to an open circuit voltage of 0.758 V. In combination with the $i$-$V$ curves in Figure 5a, this allows the prediction of the fuel cell voltage, and consequently power, at the given steady state current [21]. Figure 8 illustrates the estimated steady state

performance curves for the four catholytes, generated using the method described in Ref. [21]. The end of the curves represents the point at which all the vanadium becomes reduced to the vanadium(IV) state, i.e. the maximum steady state current density achievable for each system. Catholytes with 4 vanadium atoms per empirical formula outperform their V3 counterparts, as expected from both the cell performance and regeneration results in Figures 6 and 7, where the extra vanadium atom was advantageous. HV4 and NaV4 have similar steady state performance, with the latter having a slightly greater maximum power density of 578 mW $cm^{-2}$, which is the highest CRRC PEFC steady state power density reported to date. This comparison illustrates the trade-off between optimising cell performance and maximizing regeneration rates. The former is achieved by decreasing pH to increase cell potential, whilst increasing pH benefits the latter. Thus, catholyte pH has an important role in POM-based CRRC systems.

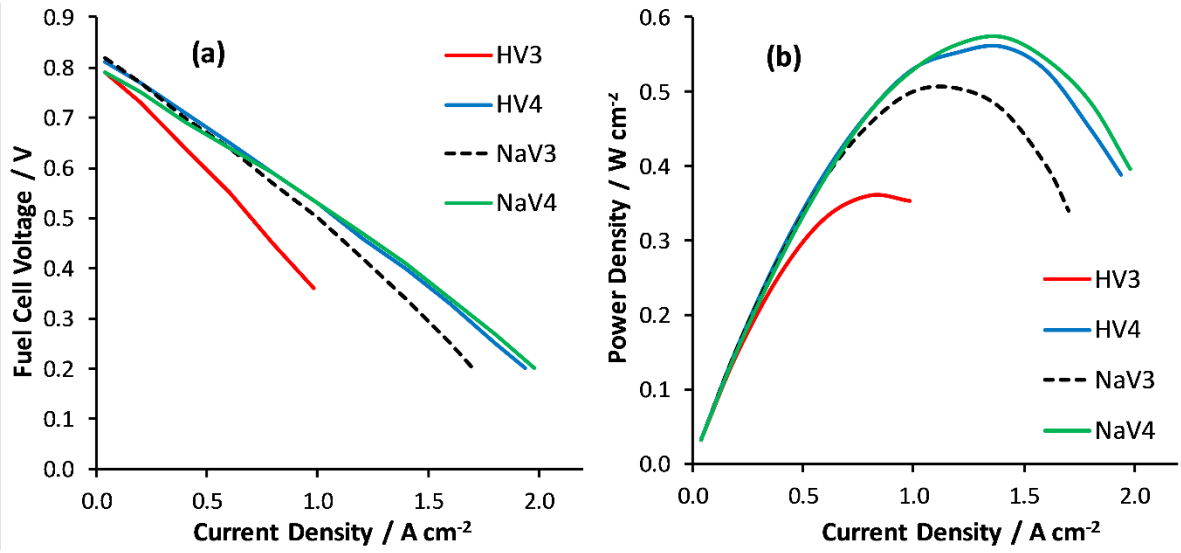


**Figure 8.** Estimated steady state (a) *i-V* and (b) power density curves for each of the four catholyte formulations.

The key performance figures from Figure 8 are listed in Table 2. The steady state performance is considerably worse than the corresponding transient performance at a reduction level of 5%, with the largest difference for the protonic POMs. Likewise, steady state performance is considerably less than the DOE targets and conventional PEFCs. A major contributing factor to the large difference between "best" and steady state performance is the effectiveness of the bubbler. For NaV4 and HV4, maximum steady state power occurred at a cell current density of 1.4 A $cm^{-2}$, corresponding to a

regeneration current of 35 A. Given the volume of catholyte in the regeneration vessel was approximately 250 mL, this corresponds to a "volumetric regeneration current density" of 140 A $L^{-1}$. Regeneration technology capable of achieving much higher volumetric regeneration current densities has been disclosed in the patent literature, where catholyte flows across a planar porous surface generating microbubbles [51]. Thus, steady state performance can be improved by bubbling technology in addition to optimizing cell performance and catholyte formulation.

A steady state durability test was performed with the most promising catholyte, NaV4 (0.3 M). A cell was operated at a discharge current of 0.4 A $cm^{-2}$ for 200 hours. Figure S4 illustrates the cell voltage over the 200-hour period. There was no loss in performance of the cell during this time indicating minimal cell degradation and good catholyte stability.

## 4. Conclusions

Four POM catholyte formulations were evaluated in a CRRC PEFC system. The catholytes varied in vanadium content (3 vs. 4 vanadium atoms per empirical formula), counter ion ($Na^+$ vs. $H^+$) and pH. In terms of cell performance, pH had the greatest effect. The redox potentials of the protonic POMs were approximately 100 mV higher than the sodium POMs for the same reduction level, resulting in higher fuel cell power densities. The number of vanadium atoms in the empirical formula only influenced fuel cell performance at high current densities, whereas the presence of sodium cations may have aided solution conductivity at high reduction levels. In addition, the cell performance of the slightly reduced catholytes was better than conventional high performance conventional PEFCs and exceeded some key DOE transportation targets, with a new record peak power density of 1.078 W $cm^{-2}$ for CRRC PEFCs (obtained with 0.3 M $H_7PV_4Mo_8O_{40}$).

In terms of regeneration performance, pH had the opposite effect, where increasing the pH of the POM favoured the presence of reduced keggin species (as opposed to free vanadium) and improved regeneration. Increasing the vanadium content of the POM also helped to increase regeneration currents, most noticeably for the protonic POMs. Thus, although increased vanadium content was

beneficial for both cell and regeneration performance, there was a trade-off for pH: NaV4 and HV4 gave very similar steady state performance, with NaV4 showing a slight advantage and setting a record peak power density of 578 mW $cm^{-2}$ for CRRC PEFC steady state operation.

Many more formulation variations are possible. These will be explored in future work to optimize the catholyte chemistry. However, when considering the general goal of maximising CRRC PEFC system performance, optimizing the catholyte formulation is only one third of the challenge. First, the regenerator needs to be both effective and efficient, achieving much higher volumetric regeneration current densities reported in this work whilst keeping the parasitic energy loss (associated with bubble production) minimal. Second, the cell requires significant optimization. For example, the work reported here used standard materials (membranes, electrodes, gas diffusion layers, etc.) optimized for flow batteries and conventional fuel cells. These components and the cell design can be further improved. Thus, CRRC PEFC systems are exciting to study as they combine inorganic chemistry, materials science, electrochemistry and chemical engineering to offer a promising and alternative solution to the major problems of PEFC cost and durability.

## 5. Acknowledgements

This study was part funded by the HEFCE (Higher Education Funding Council for England) Innovation Fund. The authors also thank Dr Corinne Wills (Newcastle University) for the NMR analysis and Dr Matthew Herbert (University of Chester), Joshua Denne (Advanced Propulsion Centre), Constantinos Menelaou (University of Chester) and Belloumi Kangati (Addivant UK Ltd) for their help and advice.

## 6. References

[1] S. Hirano, D. Papageorgopoulos, Fuel Cell Technical Team Roadmap, U.S. DRIVE (June 2013).

[2] M. Jouin, M. Bressel, S. Morando, R. Gouriveau, D. Hissel, M.-C. Péra, N. Zerhouni, S. Jemei, M. Hilairet, B. Ould Bouamama, Applied Energy, 177 (2016) 87-97.

[3] H. A. Gasteiger, N. M. Markovic, Science, 324 (2009) 48-49

[4] F. T. Wagner, B. Lakshmanan, M. F. Mathias, Journal of Physical Chemistry Letters, 1 (2010) 2204-2219.

[5] O. T. Holton, J. W. Stevenson, Platinum Metals Review, 57 (2013) 259-271.

[6] W. Gu, D. R. Baker, Y. Liu, H. A. Gasteiger, Handbook of Fuel Cells: Fundamentals, Technology and Applications, Vol. 6, p. 631–657, John Wiley & Sons, Chichester 2009.

[7] C.A. Reiser, L. Bregoli, T.W. Patterson, S.Y. Jung, J.D. Yang, M.L. Perry, T.D. Jarvi, Electrochemical and Solid-State Letters, 8 (2005) A273-A276.

[8] E. Brightman, G. Hinds, Journal of Power Sources, 267 (2014) 160-170.

[9] F.D. Coms, Ecs Transactions, 16 (2008) 235-255.

[10] E. Endoh, S. Terazono, H. Widjaja, Y. Takimoto, Electrochemical and Solid-State Letters, 7 (2004) A209-A211.

[11] Y.V. Tolmachev, M.A. Vorotyntsev, Russian Journal of Electrochemistry, 50 (2014) 403-411.

[12] A. M. Posner, Fuel, 34 (1955) 330-338.

[13] J. Kummer, D.-G. Oei, Journal of Applied Electrochemistry, 12 (1982) 87-100.

[14] J. Kummer, D.-G. Oei, Journal of Applied Electrochemistry, 15 (1985) 619-629.

[15] S.-B. Han, D.-H. Kwak, H. S. Park, I.-A. Choi, J.-Y. Park, K.-B. Ma, J.-U. Won, D.-H. Kim, S.-J. Kim, M.-C. Kim, K.-W. Park, ACS Catalysis, 6 (2016) 5302-5306.

[16] Z. Siroma, S.-i. Yamazaki, N. Fujiwara, M. Asahi, T. Nagai, Journal of Power Sources, 24 (2013) 106-113.

[17] S.-B. Han, D.-H. Kwak, H. S. Park, I.-A. Choi, J.-Y. Park, S.-J. Kim, M.-C. Kim, S. Hong, K.-W. Park, Angewandte Chemie International Edition, 56 (2017) 2893-2897.

[18] S.-B. Han, Y.-J. Song, Y.-W. Lee, A.-R. Ko, J.-K. Oh, K.-W. Park, Chemical Comunications, 47 (2011) 3496-3498.

[19] T. Matsui, E. Morikawa, S. Nakada, T. Okanishi, H. Muroyama, Y. Hirao, T. Takahashi, K. Eguchi ACS Applied Materials & Interfaces, 8 (2016) 18119-18125

[20] R. Singh, A.A. Shah, A. Potter, B. Clarkson, A. Creeth, C. Downs, F.C. Walsh, Journal of Power Sources, 201 (2012) 159-163

[21] N. L. O. Gunn, D. B. Ward, C. Menelaou, M. A. Herbert, T. J. Davies, Journal of Power Sources, 348 (2017) 107-117.

[22] http://www.fuelcelltoday.com/news-archive/2013/june/acal-energy-fuel-cell-achieves-10,000-hour-endurance

[23] H. A. Gasteiger, S. S. Kocha, B. Sompalli, F. T. Wagner, Applied Catalysis B: Environmental, 56 (2005) 9-35.

[24] A. Creeth, Fuel Cells Bulletin, 2011 (2011) 12-15.

[25] J. J. Borrás-Almenar, E. Coronado, A. Müller, M. Pope, Polyoxometalate molecular science, Springer Science & Business Media, 2003.

[26] L. Pettersson, Molecular Engineering, 3 (1993) 29-42.

[27] L. Pettersson, I. Andersson, A. Selling, J. H. Grate, Inorganic Chemistry, 33 (1994) 982-993.

[28] A. Selling, I. Andersson, J. H. Grate, L. Pettersson, European Journal of Inorganic Chemistry, (2000) 1509-1521.

[29] I. V. Kozhevnikov, Chemical Reviews, 98 (1998) 171-198.

[30] V. Odyakov, E. Zhizhina, K. Matveev, Journal of Molecular Catalysis A: Chemical, 158 (2000) 453-456.

[31] E. Zhizhina, V. Odyakov, M. Simonova, K. Matveev, Kinetics and catalysis, 46 (2005) 354-363.

[32] E. Zhizhina, V. Odyakov, M. Simonova, K. Matveev, Reaction Kinetics and Catalysis Letters, 78 (2003) 373-379.

[33] I. V. Kozhevnikov, Izvestiya Akademii Nauk SSSR: Seriya Khimicheskaya, 4 (1983) 721-726.

[34] N. Martin, M. Herbert, Synthesis of Polyoxometalates, WO2015/097459 A1.

[35] T. J. Davies, J. Denne, N. B. Baynes, Redox Probe, GB 2527104 (A).

[36] P. Souchay, F. Chauveau, P. Courtin, Bulletin De La Societe Chimique De France, (1968) 2384-2389.

[37] https://energy.gov/sites/prod/files/2017/05/f34/fcto_myrdd_fuel_cells.pdf

[38] R. O'Hayre, S.-W. Cha, W. Colella, F. B. Prinz, Fuel Cell Fundamentals, second edition, Wiley, New York, 2009, chapter 9.

[39] D. Chen, M.A. Hickner, E. Agar, E.C. Kumbur, Journal of Membrane Science, 437 (2013) 108-113.

[40] D.S. Aaron, Q. Liu, Z. Tang, G.M. Grim, A.B. Papandrew, A. Turhan, T.A. Zawodzinski, M.M. Mench, Journal of Power Sources, 206 (2012) 450-453.

[41] Q.H. Liu, G.M. Grim, A.B. Papandrew, A. Turhan, T.A. Zawodzinski, M.M. Mench, Journal of the Electrochemical Society, 159 (2012) A1246-A1252.

[42] J. Houser, A. Pezeshki, J.T. Clement, D. Aaron, M.M. Mench, Journal of Power Sources, 351 (2017) 96-105.

[43] X.L. Zhou, T.S. Zhao, L. An, Y.K. Zeng, L. Wei, Journal of Power Sources, 339 (2017) 1-12.

[44] X.L. Zhou, T.S. Zhao, Y.K. Zeng, L. An, L. Wei, Journal of Power Sources, 329 (2016) 247-254.

[45] X.L. Zhou, Y.K. Zeng, X.B. Zhu, L. Wei, T.S. Zhao, Journal of Power Sources, 325 (2016) 329-336.

[46] K.T. Cho, P. Albertus, V. Battaglia, A. Kojic, V. Srinivasan, A.Z. Weber, Energy Technology, 1 (2013) 596-608.

[47] V. M. Berdnikov, L. I. Kuznetsova, K. I. Matveev, N. P. Kirik, E. N. Yurchenko, Koordinatsionnaya Khimiya, 5 (1979) 78-85.

[48] I. V. Kozhevnikov, Yu. V. Burov, K. I. Matveev, Izvestiya Akademii Nauk SSSR, Seriya Khimicheskaya, 11 (1981) 2428-2435.

[49] L. N. Kuznetsova, E. N. Yurchenko, R. I. Maksimovskaya, N. P. Kirik, K. I. Matveev, Koordinatsionnaya Khimiya, 3 (1977) 51-58.

[50] A. Selling, I. Andersson, J. H. Grate, L. Pettersson, European Journal of Inorganic Chemistry, (2002) 743-749.

[51] R. Longman, B. Clarkson, Bubbles Generation Device and Method, WO 2011/107795 A2.

## Tables

**Table 1**: Target vanadium(IV) fractions and corresponding fuel cell open circuit voltages at 80°C.

| V fraction as V(IV) | Cell Open Circuit Voltage* / mV | | | |
|---|---|---|---|---|
| | HV3 | HV4 | NaV3 | NaV4 |
| 0.05 | 997 | 1010 | 935 | 905 |
| 0.25 | 925 | 920 | 798 | 793 |
| 0.45 | 854 | 835 | 745 | 747 |
| 0.65 | 776 | 755 | 708 | 714 |
| 0.85 | 728 | 710 | 650 | 675 |

* vs. $H_2$-Pt anode

**Table 2**: Comparison of CRRC PEFC performance using four different catholytes (last eight rows) with previously reported results from CRRC and conventional PEFCs and selected Department of Energy targets.

| System | Catholyte | OCV / mV | Pt Loading / mg $cm^{-2}$ | Performance @ 0.8 V / mA $cm^{-2}$ | Cell Voltage at 0.2 A $cm^{-2}$ / mV | Cell Voltage at 1 A $cm^{-2}$ / mV | Max Power / mW $cm^{-2}$ | High Frequency Resistance / mΩ $cm^2$ | Ref. |
|---|---|---|---|---|---|---|---|---|---|
| DOE 2020 Targets | - | - | 0.125 | 300 | - | - | 1000 | - | [37] |
| Conventional PEFC (Pt Cathode) | Air | 960 | 0.80 | 210 | 810 | 670 | >830 | 45-55 | [23] |
| CRRC PEFC | 0.3 M HV3 @ 0.05 V(IV) | 990 | 0.40 | - | 900 | 720[b] | 1000 | - | [21] |
| CRRC PEFC | 0.3 M HV3 @ steady state) | 820 | 0.40 | - | 730 | 370 | 380 | 173 | [21] |
| Present work (C cathode) | 0.3 M HV3 @ 0.05 V(IV) | 993 | 0.40 | 586 | 904 | 700 | 1004 | 119[b] | |
| Present work (C cathode) | 0.3 M HV3 @ steady state) | 810[a] | 0.40 | - | 733 | - | 363 | - | |
| Present work (C cathode) | 0.3 M HV4 @ 0.05 V(IV) | 1013 | 0.40 | 708 | 927 | 736 | 1078 | 120[b] | |
| Present work (C cathode) | 0.3 M HV4 @ steady state) | 820[a] | 0.40 | 85 | 772 | 532 | 566 | - | |
| Present work (C cathode) | 0.3 M NaV3 @ 0.05 V(IV) | 932 | 0.40 | 284 | 834 | 623 | 869 | 108[b] | |
| Present work (C cathode) | 0.3 M NaV3 @ steady state) | 835[a] | 0.40 | 116 | 772 | 501 | 509 | - | |
| Present work (C cathode) | 0.3 M NaV4 @ 0.05 V(IV) | 902 | 0.40 | 224 | 809 | 606 | 864 | 103[b] | |
| Present work (C cathode) | 0.3 M NaV4 @ steady state) | 802[a] | 0.40 | - | 752 | 532 | 578 | - | |

a Extrapolated to zero current from Figure 8a
b Measured @ 0.65 V(IV)